

Supporting Information

Efficient Room-Temperature Phosphorescence Based on Pure Organic Sulfur-Containing Heterocycle: Folding-Induced Spin-Orbit Coupling Enhancement

*Haichao Liu,^{a,+} Yu Gao,^{a,+} Jungang Cao,^b Tingxuan Li,^b Yating Wen,^a Yunpeng Ge,^a Lili Zhang,^b Guocui Pan,^b Tong Zhou^b and Bing Yang^{*a}*

^a State Key Laboratory of Supramolecular Structure and Materials, College of Chemistry, Jilin University, Changchun, 130012, P. R. China

^b College of Chemistry, Jilin University, Changchun, 130012, P. R. China

⁺ Haichao Liu and Yu Gao contributed equally to this work.

*Corresponding Author E-mail: yangbing@jlu.edu.cn

SI Experimental details

SI-1 General information: All the solvents used for the synthesis were purchased from Aldrich company and used without further purification. ^1H and ^{13}C NMR spectra were recorded on a Bruker AVANCE 500 spectrometer, using tetramethylsilane (TMS) as the internal standard. The GC-MS mass spectra were recorded using Thermo Fisher ITQ1100 instrument. The compounds were characterized by a Flash EA 1112, CHNS elemental analysis instrument.

SI-2 Single crystal X-ray diffraction (XRD) data: Single crystals of TA, 1TA2TA and 1TA1TA were prepared by crystallization from dichloromethane:methanol (2:1, v/v) mixture at room temperature. The diffraction experiments were carried out on a Rigaku R-AXIS RAPID diffractometer equipped with a Mo- $\text{K}\alpha$ and control Software using the RAPID AUTO at 293 (± 2) °C. The crystal structures were solved with direct methods and refined with a full-matrix least-squares technique using the SHELXS programs. Powder XRD patterns were collected on a Rigaku SmartLab(3) diffractometer.

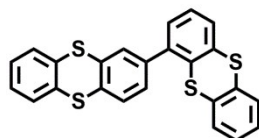
SI-3 Photophysical measurements: UV-vis spectra of solutions and films were recorded on a Shimadzu UV-3100 Spectrophotometer. Steady-state photoluminescence (PL) spectra and lifetimes were carried out with FLS980 Spectrometer. Quantum efficiencies were measured using an integrating sphere apparatus. Solutions were placed in 1 cm path length quartz cells, and crystals were fixed on the quartz plate in terms of steady-state spectra and lifetimes.

SI-4 Theoretical calculation: All the density functional theory (DFT) calculations were carried out using Gaussian 09 (version D.01) package on a Power Leader cluster. Single molecular structure of TA was directly taken out from crystal structures to calculate excited-state energies and spin-orbit coupling (SOC) coefficients. The absorption properties were obtained using TD-cam-b3lyp/6-31g(d, p) at the ground state geometries. In order to examine the nature of electronic transitions for excited-states, natural transition orbitals (NTOs) are evaluated with the dominant “particle”-“hole” pair contributions. SOC coefficients were calculated based on cam-b3lyp/6-31g(d, p) in Beijing Density Function (BDF) software.

SI-5 Thermal stability measurements: Thermal gravimetric analysis (TGA) was undertaken on a PerkinElmer thermal analysis system at a heating rate of 10 °C min⁻¹ and a nitrogen flow rate of 80 mL min⁻¹. Differential scanning calorimetry (DSC) analysis was carried out using a NETZSCH (DSC-204) instrument at 10 °C min⁻¹ while flushing with nitrogen.

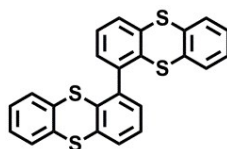
S II The details of synthetic procedures

TA sample was purchased from J&k company and further purified by sublimation method. Single crystal was grown in the dichloromethane/methanol mixture by solvent diffusion method, and colorless block crystals were obtained. ^1H NMR (500 MHz, DMSO, 25 °C, TMS): δ 7.59 (dd, $J = 5.0, 3.6$ Hz, 4H), 7.36 (dd, $J = 5.0, 3.5$ Hz, 4H); ^{13}C NMR (126 MHz, CDCl_3 , 25 °C, TMS): $\delta = 135.58$ (C), 128.76 (CH), 127.71 (CH); GC-MS, EI, mass m/z : 216.06; Anal. calcd for $\text{C}_{12}\text{H}_8\text{S}_2$: C 66.63, H 3.73, S 29.64; found: C 66.79, H 3.78, S 29.35.



Compound 1TA2TA: 1,2'-bithianthrene

The synthesis of compound 1TA2TA was referring to Ref. 1.^[1]



Compound 1TA1TA: 1,1'-bithianthrene

The synthesis of compound 1TA1TA was referring to Ref. 1.^[1]

SIII Figures

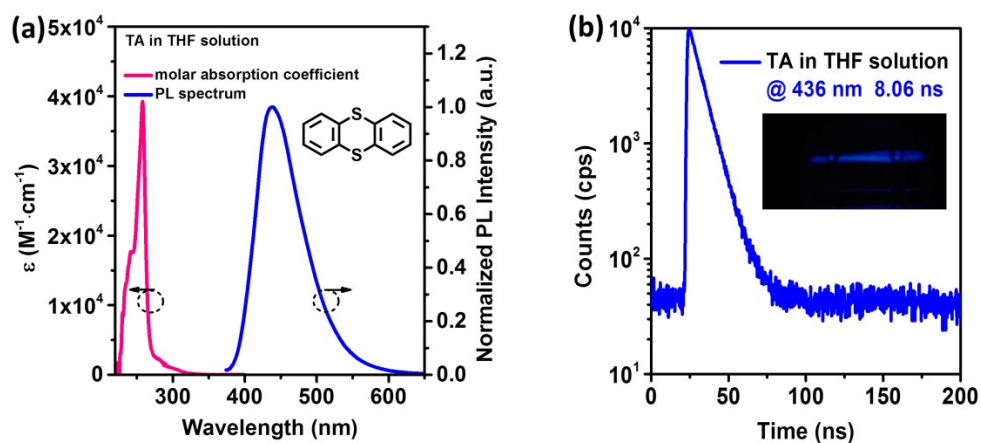


Figure S1. (a) Molar absorption coefficient and PL spectrum of TA in THF solution. (b) Time-resolved spectrum of TA in THF solution.

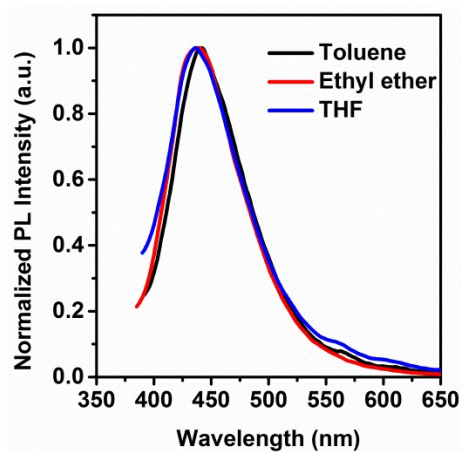


Figure S2. PL spectra of TA in different solvents.

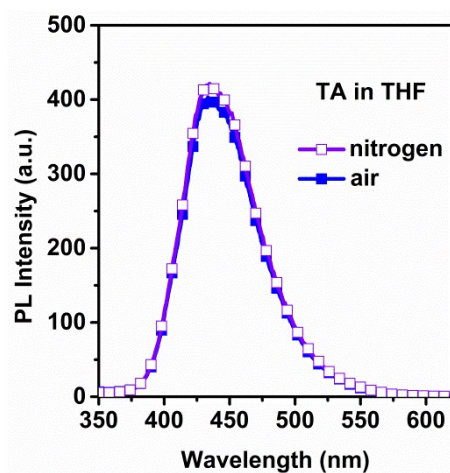


Figure S3. PL spectra of TA in THF solution at room temperature in air and nitrogen atmospheres, respectively.

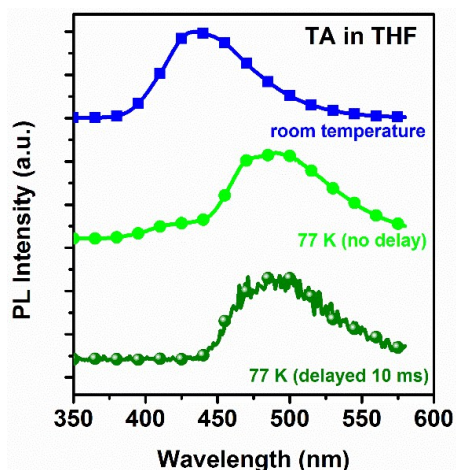


Figure S4. PL spectra of TA in THF solution at room temperature and 77 K. In frozen THF solution (10 μM) at 77 K, TA demonstrates the strong emission with the maximum intensity at wavelength of 490 nm, together with a shoulder emission band around 430 nm. After delayed 10 ms, TA only shows one emission band peaking at 490 nm, which could be identified as phosphorescence emission. Emission band around 430 nm should be assigned to the fluorescent characteristic, which is blue-shifted relative to that in THF solution at room temperature. This blue-shift can probably result from the restricted vibration relaxation of TA in rigid frozen state.

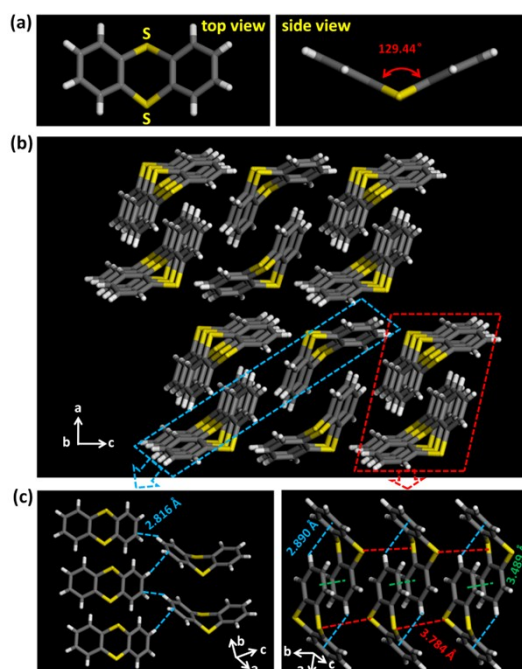


Figure S5 (a) Molecular conformation of TA in crystal structure. (b) Crystal stacking structure of TA. (c) Intermolecular interactions in TA crystal. In crystal structure, TA presents the folded molecular geometry with a dihedral angle of 129.44° . These folded molecules closely pack together and regular arrangement is observed along with b axis. Short contact occurs between carbon and hydrogen atoms with the distance of 2.816 \AA . Dimer structures were obviously observed, and there are strong $\text{C-H}\cdots\pi$ (2.890 \AA) and π - π (3.489 \AA) interactions between two TA molecules in dimer. Moreover, continuous weak sulfur...sulfur ($\text{S}\cdots\text{S}$) interactions exist between the two adjacent molecules with the distance of 3.784 \AA .

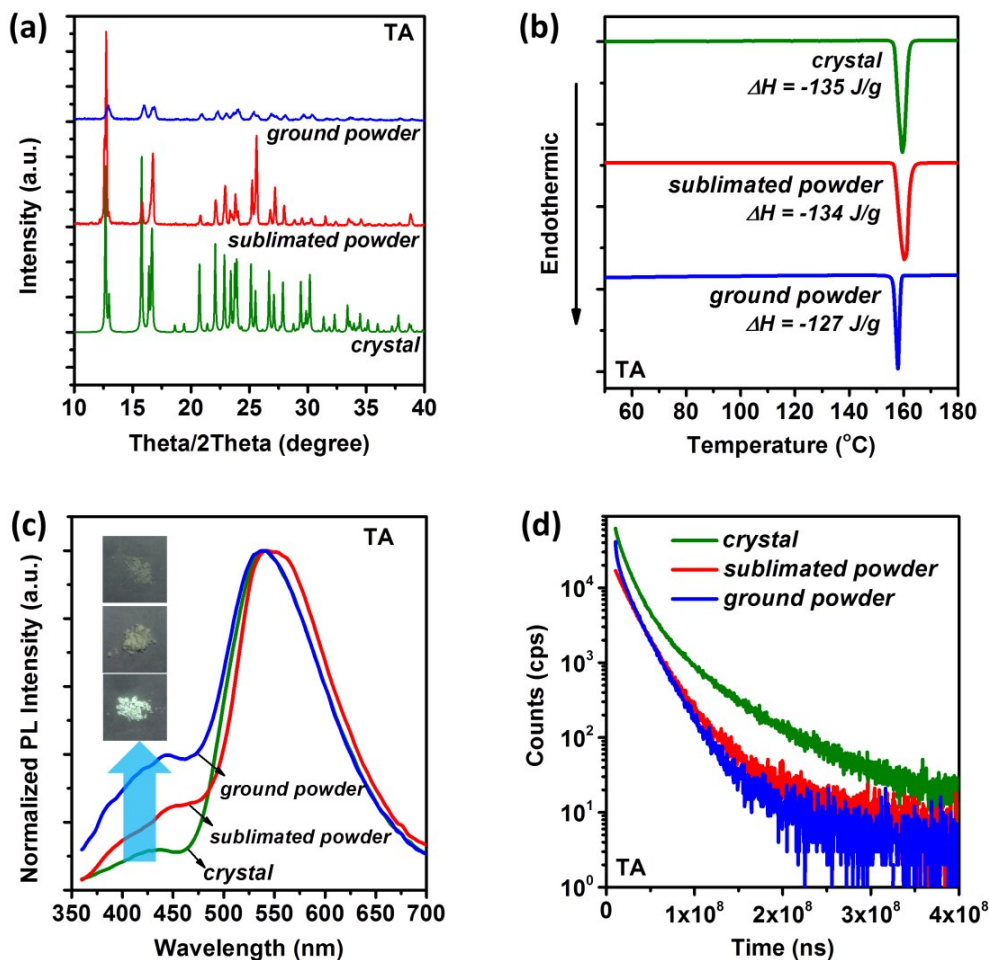


Figure S6. (a) Powder XRD patterns, (b) DSC curves, (c) PL spectra and (d) time-resolved spectra of crystal, sublimation powder and ground powder of TA.

TA powder shows the broad PL spectrum peaking at 540 nm with a weak emission band in blue region. Time-resolved experiment reveals a long-lived decay of TA powder at 540 nm up to millisecond (1.09 ms@9.18%, 15.89 ms@74.46%, 38.64 ms@16.36%) and very short lifetime at 430 nm (0.66 ns@80.34%, 4.18 ns@19.66%) corresponding to phosphorescence and fluorescence, respectively. TA crystal under UV irradiation demonstrates the brighter green emission relative to that of powder, and it presents a broad PL spectrum peaking at 540 nm with a weak emission band in blue region. Furthermore, TA crystal displays the visible afterglow by naked eye. Time-resolved fluorescence reveals a long-lived decay of TA crystal at 540 nm up to 23.6 ms (5.75 ms@15.26%, 16.08 ms@61.20%, 54.71 ms@23.54%) and a prompt decay at 430 nm with 1.75 ns (0.44 ns @ 79.10%, 6.73 ns @ 20.90%), which are also assigned to phosphorescence and fluorescence emission, respectively.

TA crystal exhibits the stronger phosphorescence emission and longer lifetime than those of its powder, which can be inferred that the strength of TA phosphorescence in solid state is dependent on the degree of crystallization. To confirm this point, we further ground the TA powder for 30 minutes to disorder the crystal stacking and to see if there is any change in photophysical properties. It is almost impossible to obtain the totally amorphous powder by grinding process, probably due to too strong intermolecular interactions in TA crystal. Although both sublimated powder and ground powder have identical Bragg diffraction peaks in powder XRD experiment, DSC measurement reveals the decreased

melting enthalpy from crystal (-135 J/g), sublimated powder (-134 J/g) to ground powder (-127 J/g), indicating the gradually decreased degree of TA crystallinity. As the crystallinity decreases, TA shows the gradually growing emission band in short-wavelength (fluorescence) region from crystal, sublimated powder to ground powder in normalized PL spectra with the same emission band around 540 nm. Interestingly, the ground powder shows the shorter lifetime (1.38 ms@7.10%, 11.83 ms@52.58%, 25.16 ms@40.32%) relative to those of crystal and sublimated powder. We further measured the PL efficiencies (η_{PL}) of three samples (collecting the whole spectra), and their η_{PL} s reveal a gradual decrease from crystal (25%), sublimated powder (11%) to ground powder (8%). Therefore, the crystallization exactly plays a crucial role in the efficient RTP in TA crystal.

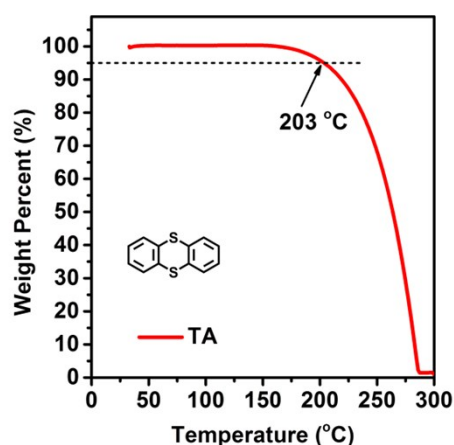


Figure S7. TGA curve of TA powder.

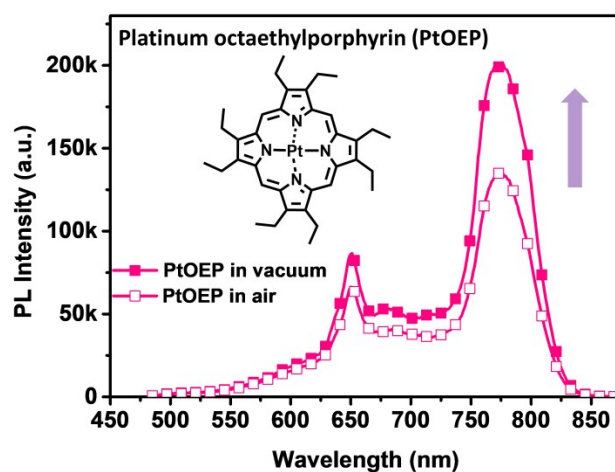


Figure S8. PL spectra of PtOEP powder in air and vacuum environment, respectively. PtOEP emitting light from triplet excitons, is sensitive to oxygen, that is, the presence of oxygen can quench the triplet excitons.

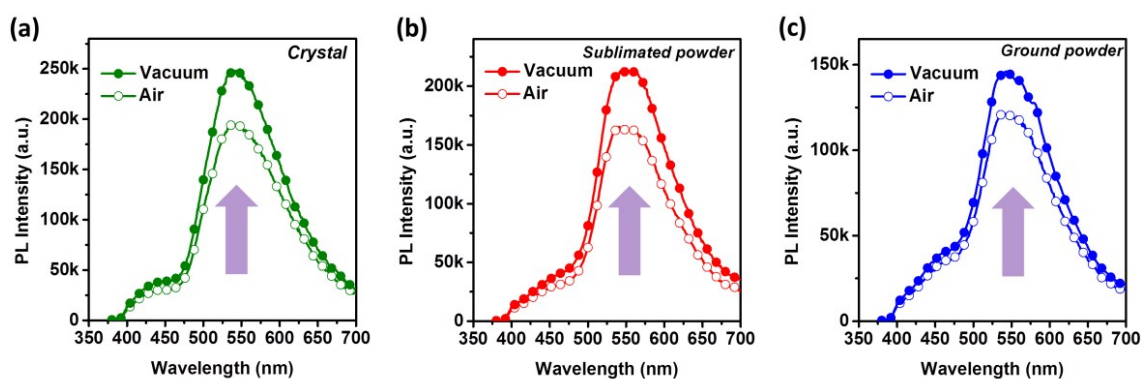


Figure S9. PL spectra of (a) crystal, (b) sublimated powder and (c) ground powder of TA in air and vacuum environment. PL spectra of TA solids (crystal, sublimated powder and ground powder) were examined in situ in the absence or presence of oxygen. Once in the vacuum (degassing) condition, all three TA solids show the much stronger emission band than those in oxygen atmosphere. These results further confirm the phosphorescence emission characteristic of TA, which is sensitive to oxygen quenching. As mentioned above, TA powder emission is weakened greatly after grinding operation, which can also be attributed to the enlarged contact surface of the ambient oxygen. Thus, crystallization process works for high-efficiency RTP of TA in two ways, *i.e.*, the greatly suppressed non-radiative vibrational quenching and the prevention the oxygen from the non-radiative energy transfer.

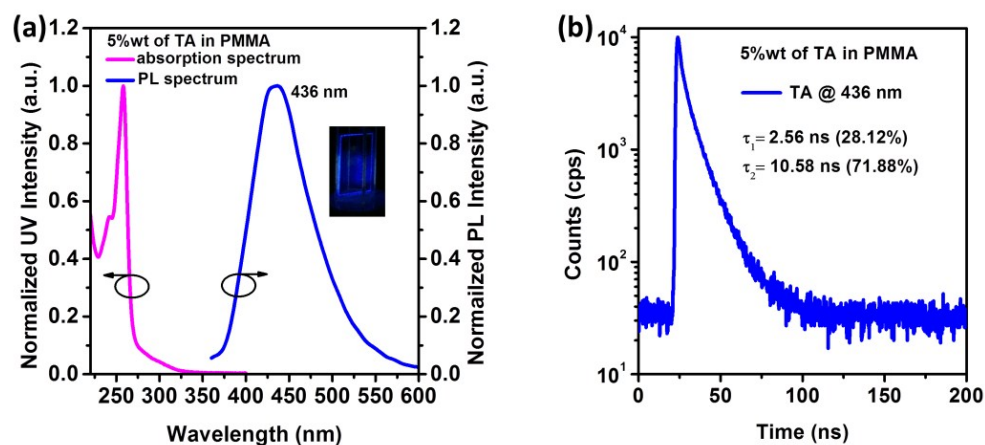


Figure S10. (a) Absorption and PL spectrum and (b) time-resolved spectrum of 5%wt of TA in PMMA film.

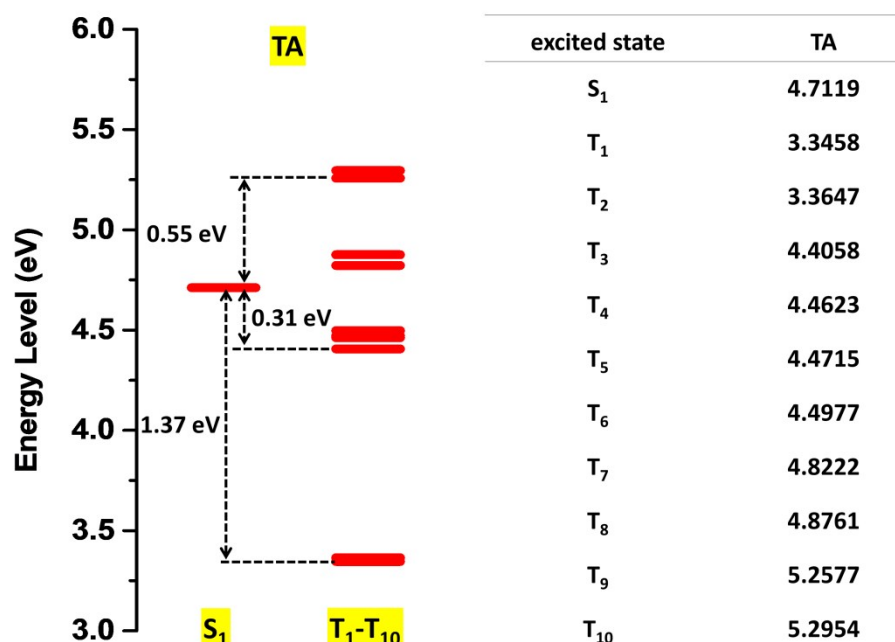


Figure S11. Diagram of energy levels of TA.

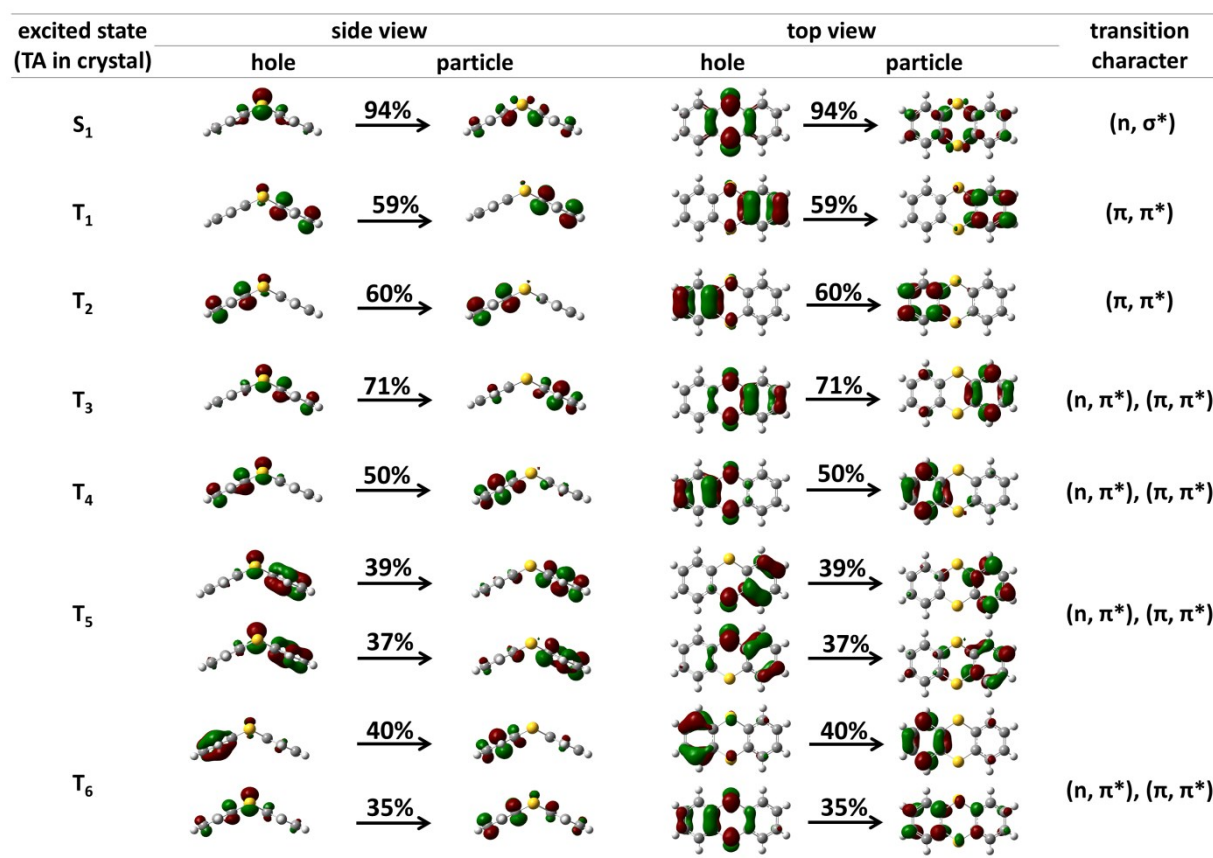


Figure S12. NTOs for $S_0 \rightarrow S_1$ transition in TA. The percentage weights of hole-particle are given for the $S_0 \rightarrow S_1$ transition.

Optimized geometries of TA

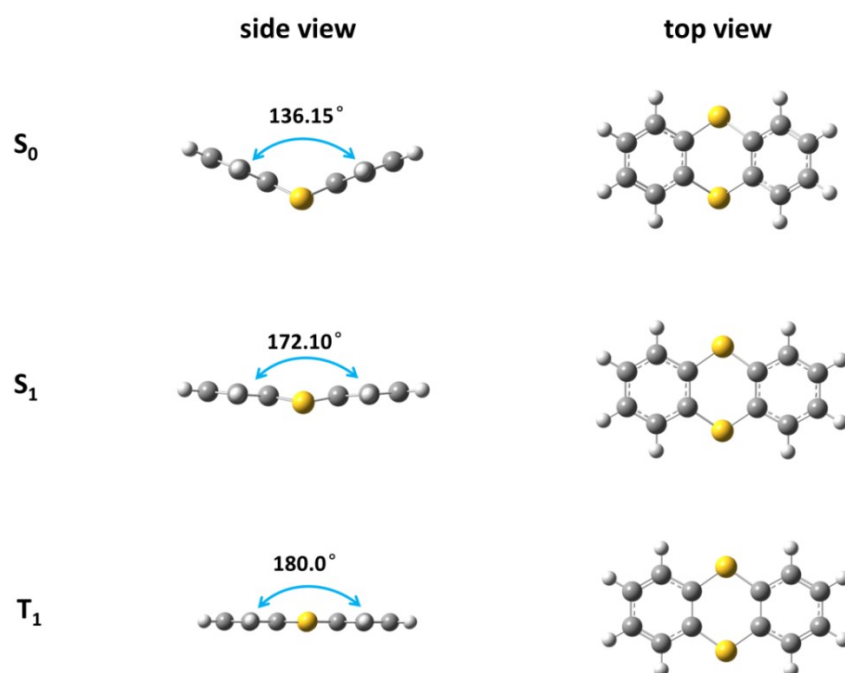


Figure S13. Optimized S_0 , S_1 and T_1 geometries of TA by Gaussuian09 software.

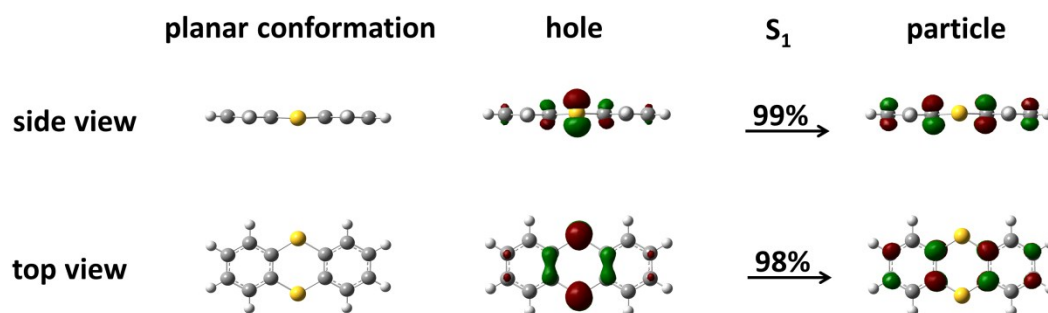


Figure S14. NTOs of TA with planar conformation for $S_0 \rightarrow S_1$ transition. The planar TA molecule (TA_{180°) is factitiously constructed by Gaussuian09 software.

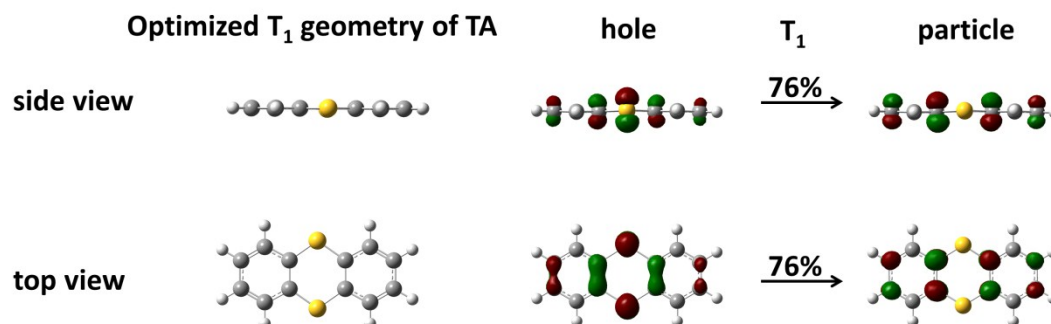


Figure S15. Optimized T_1 geometry of TA and natural transition orbital (NTO) for $T_1 \rightarrow S_0$ transition.

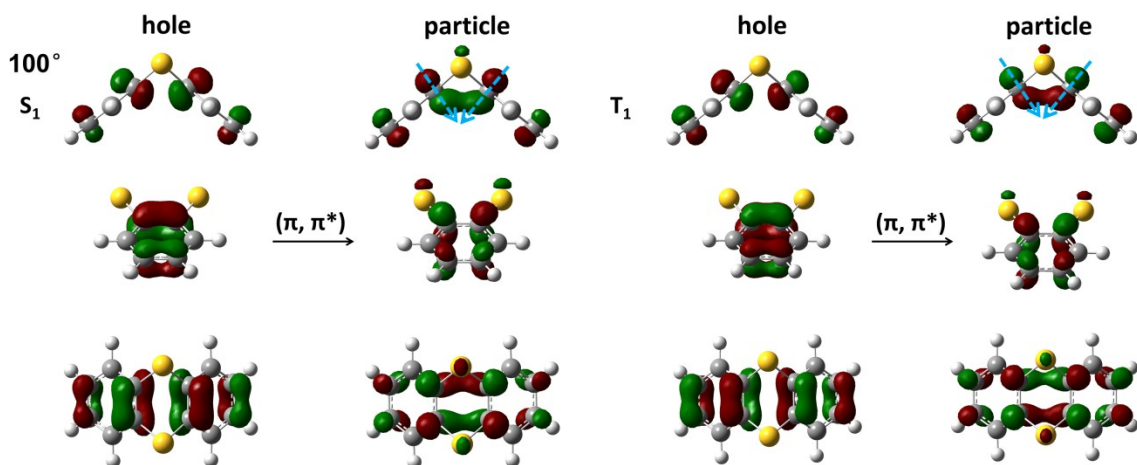


Figure S16. NTOs of TA with 100° dihedral angle based on the ground-state geometry. 100° dihedral angle is constructed by manually modulating TA conformation in crystal. Three views (side, long and top view) are shown in order.

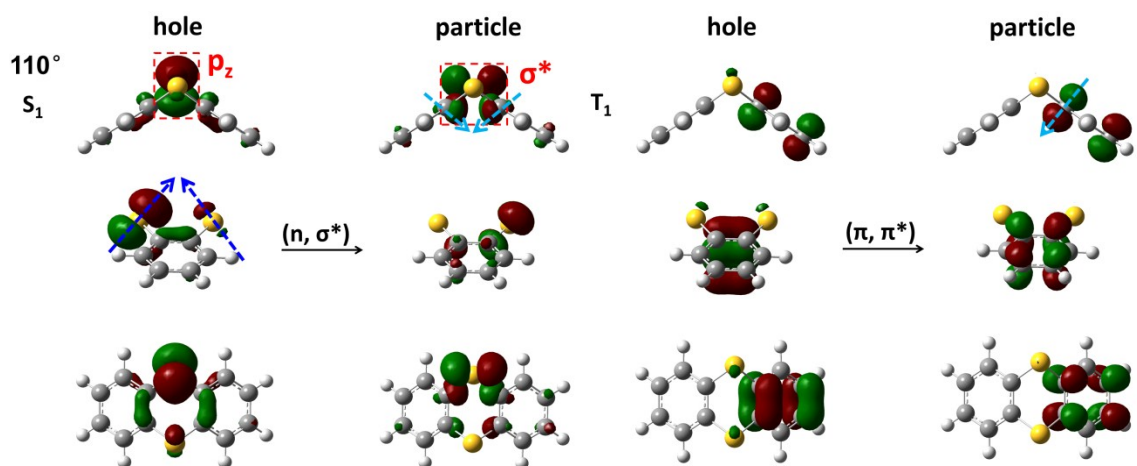


Figure S17. NTOs of TA with 110° dihedral angle based on the ground-state geometry. 110° dihedral angle is constructed by manually modulating TA conformation in crystal.

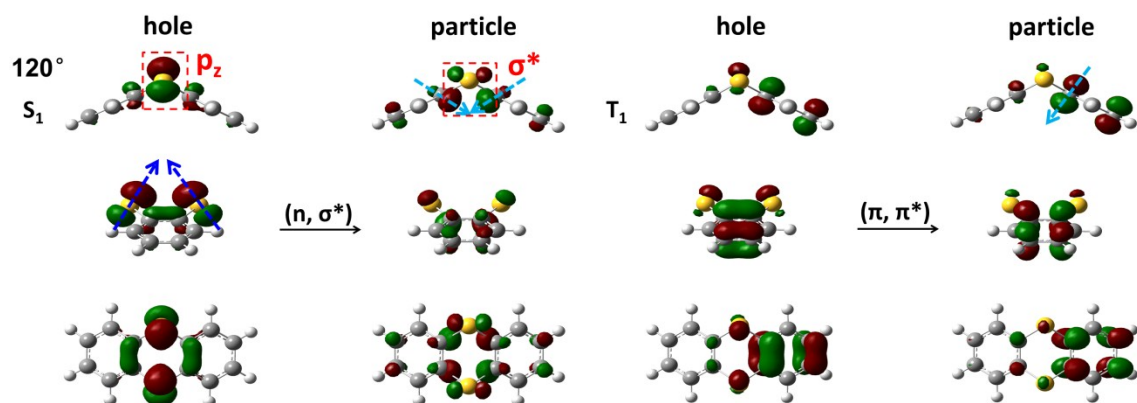


Figure S18. NTOs of TA with 120° dihedral angle based on the ground-state geometry. 120° dihedral angle is constructed by manually modulating TA conformation in crystal.

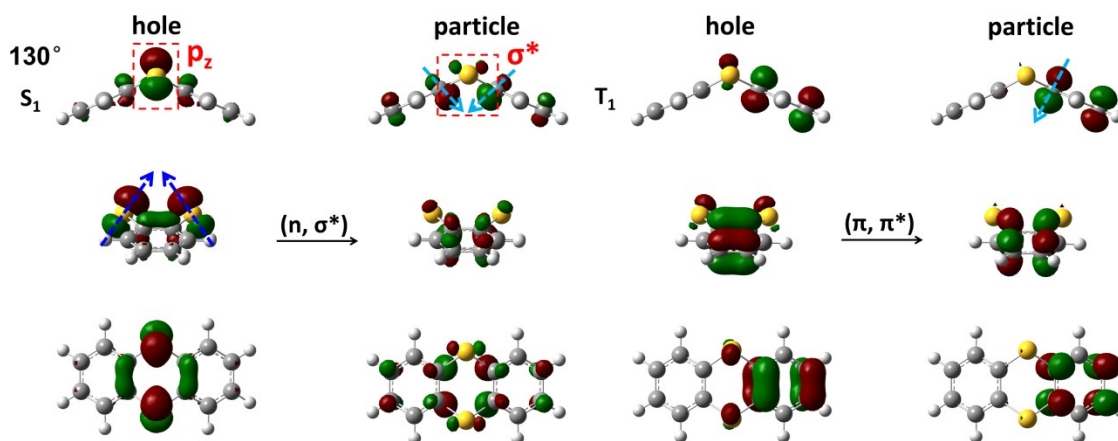


Figure S19. NTOs of TA with 130° dihedral angle based on the ground-state geometry. 130° dihedral angle is constructed by manually modulating TA conformation in crystal.

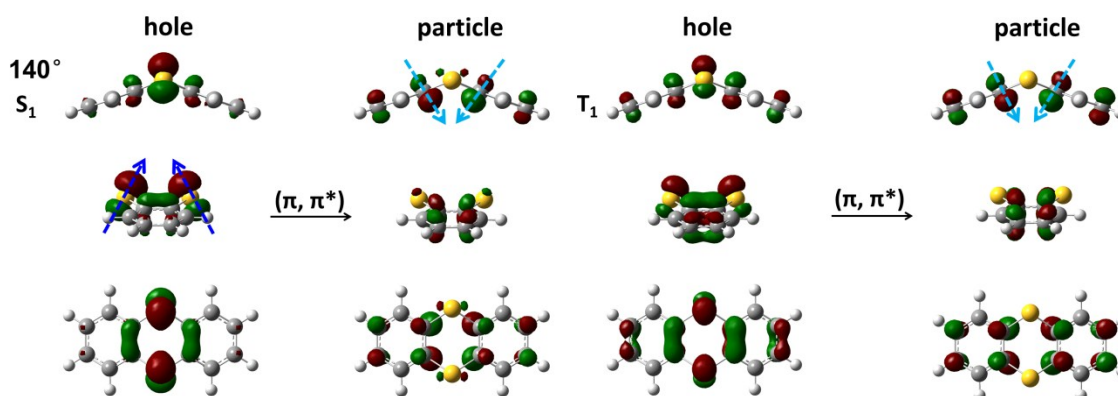


Figure S20. NTOs of TA with 140° dihedral angle based on the ground-state geometry. 140° dihedral angle is constructed by manually modulating TA conformation in crystal. In the particle of $S_0 \rightarrow S_1$ transition, p_x -orbital is not obviously extruded and thus S_1 exhibits the π - π^* transition configuration that does not play a positive role in SOC effect.

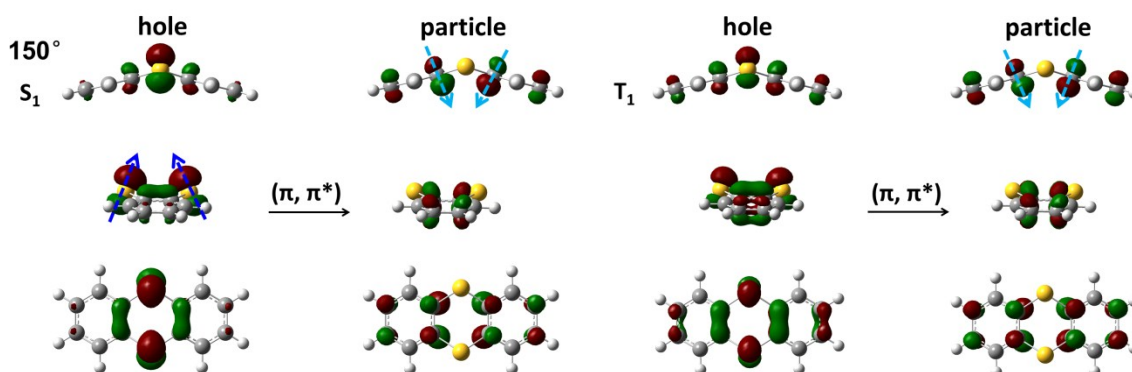


Figure S21. NTOs of TA with 150° dihedral angle based on the ground-state geometry. 150° dihedral angle is constructed by manually modulating TA conformation in crystal.

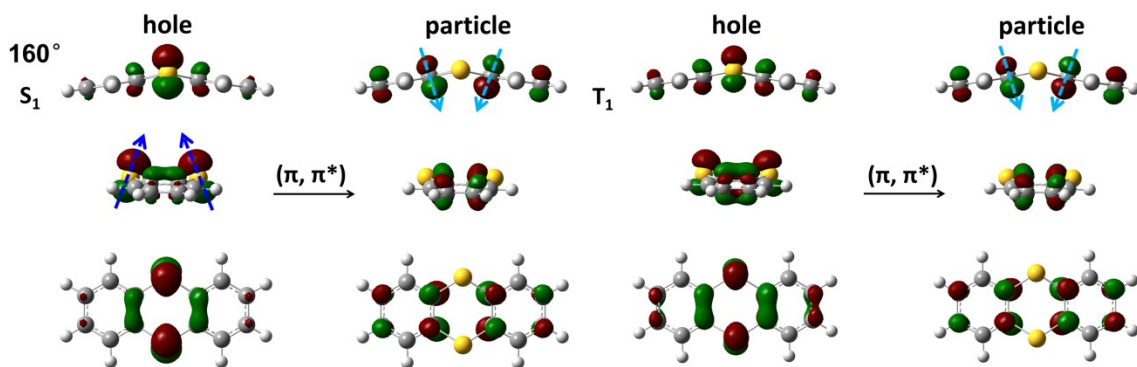


Figure S22. NTOs of TA with 160° dihedral angle based on the ground-state geometry. 160° dihedral angle is constructed by manually modulating TA conformation in crystal.

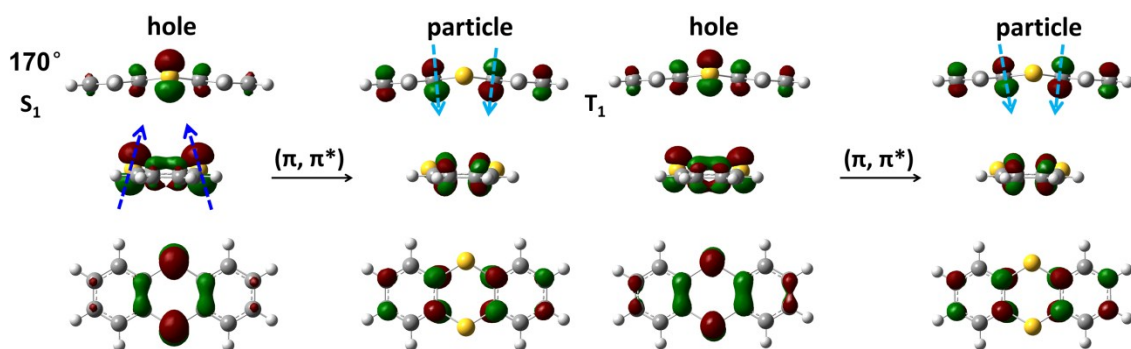


Figure S23. NTOs of TA with 170° dihedral angle based on the ground-state geometry. 170° dihedral angle is constructed by manually modulating TA conformation in crystal.

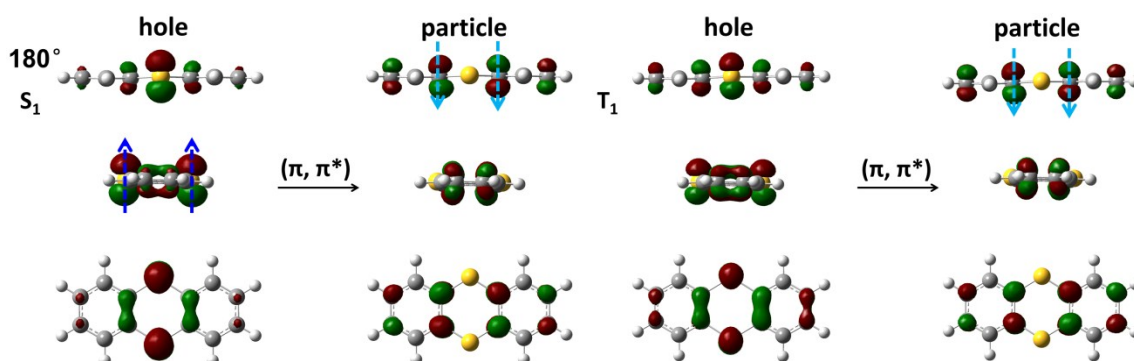


Figure S24. NTOs of TA with 180° dihedral angle based on the ground-state geometry. 180° dihedral angle is constructed by manually modulating TA conformation in crystal.

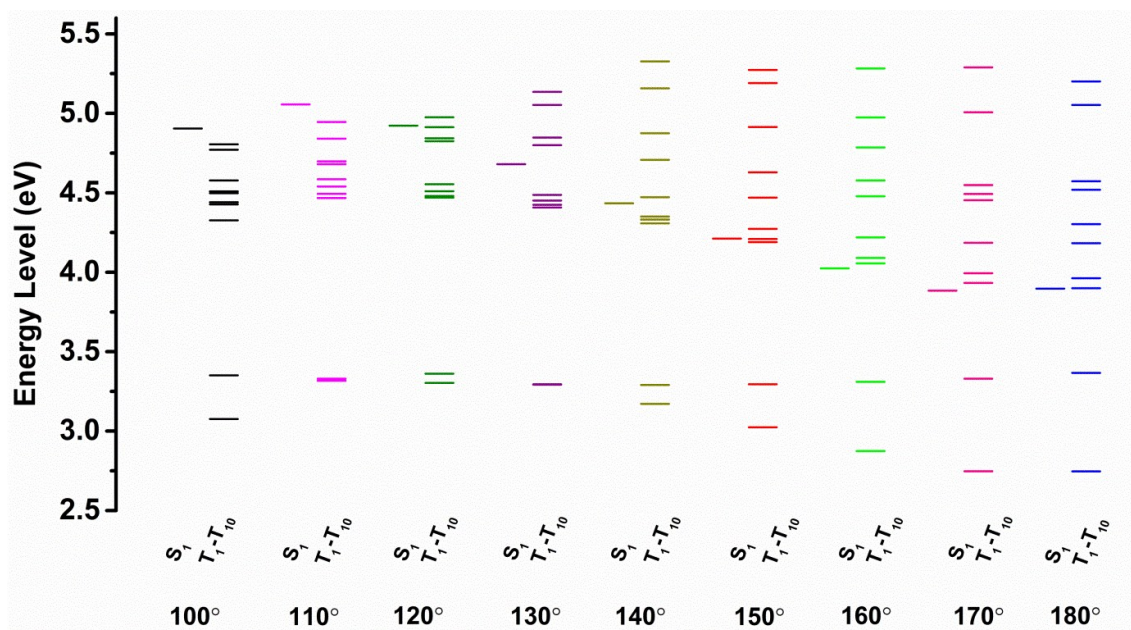


Figure S25. Diagram of energy levels of TA with different angles which are constructed by manually modulating molecular geometry in crystal.

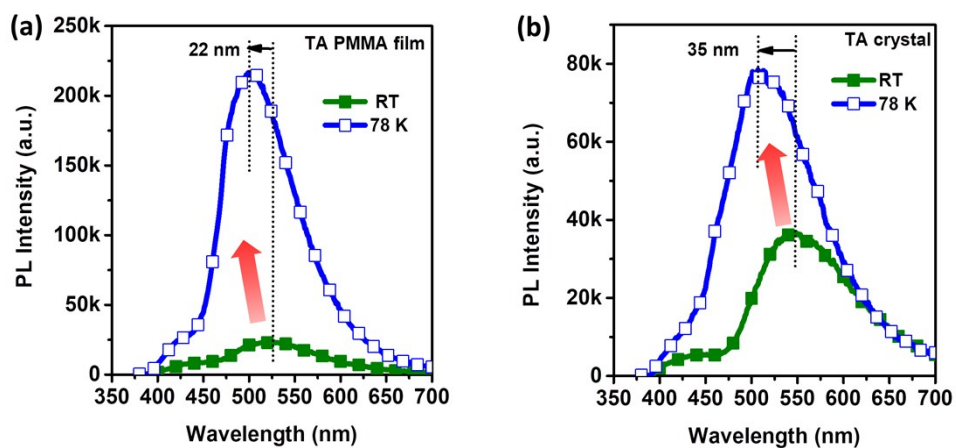


Figure S26. PL spectra of (a) TA crystal and (b) TA-PMMA doped film at RT and 78 K.

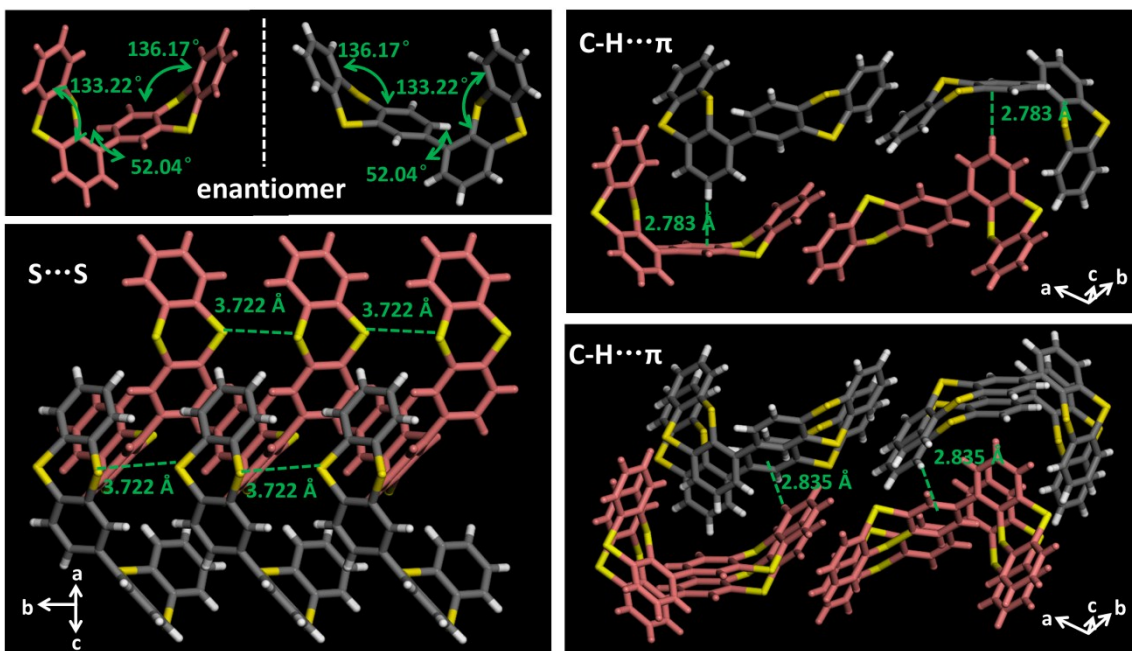


Figure S27. Molecular conformation and intermolecular interactions of 1TA2TA in crystal.

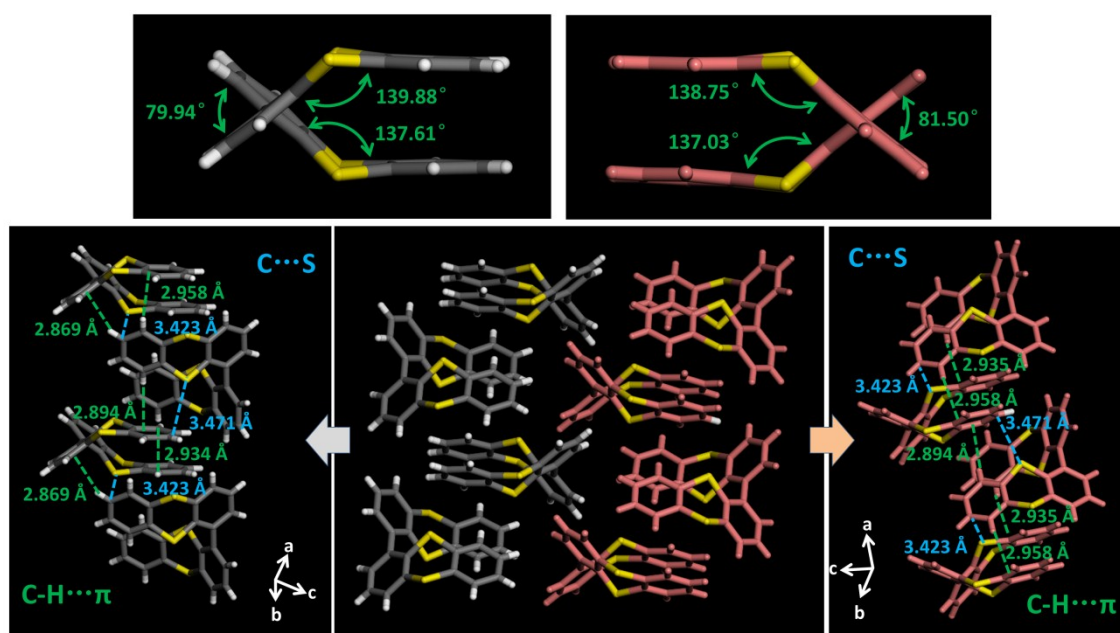


Figure S28. Molecular conformation and intermolecular interactions of 1TA1TA in crystal.

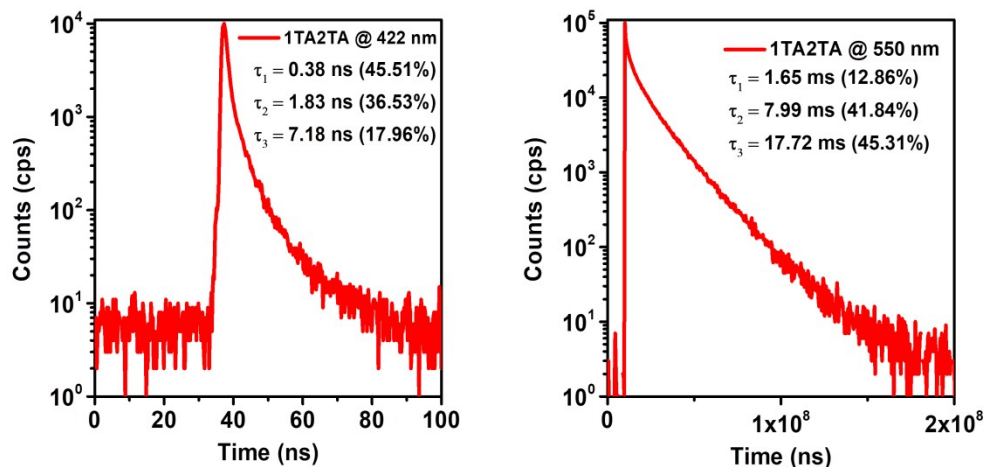


Figure S29.. Time-resolved spectra of 1TA2TA crystal.

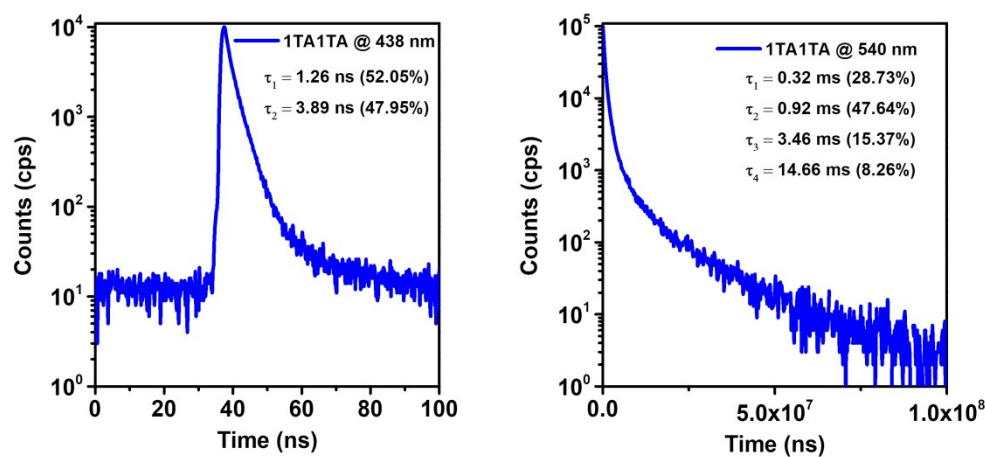


Figure S30. Time-resolved spectra of 1TA1TA crystal.

SIV Tables

Table S1. Crystallographic data for TA, 1TA2TA and 1TA1TA.

	TA	1TA2TA	1TA1TA
crystal color	colorless	colorless	colorless
empirical formula	C ₁₂ H ₈ S ₂	C ₂₄ H ₁₄ S ₄	C ₂₄ H ₁₄ S ₄
formula weight	216.30	430.59	430.59
T [K]	293(2)	296(2)	293(2)
crystal system	monoclinic	monoclinic	triclinic
space group	P 21/c	P 21/c	P -1
a [Å]	11.941(2)	23.376(5)	10.151(2)
b [Å]	6.1614(12)	6.0798(12)	10.193(2)
c [Å]	14.500(3)	14.364(3)	21.148(4)
α [°]	90.00	90.00	97.15(3)
β [°]	109.93(3)	99.514(5)	97.60(3)
γ [°]	90.00	90.00	111.09(3)
V [Å ³]	1003.0(3)	2013.4(7)	1988.4(7)
Z	4	4	4
F(000)	448	888	888
density [g/cm ³]	1.432	1.421	1.438
μ [mm ⁻¹]	0.481	0.479	0.485
reflections collected	8916	14316	19334
unique reflections	2294	4942	8968
R (int)	0.0210	0.0533	0.0421
GOF	1.076	1.018	1.086
R ₁ [I>2 σ (I)]	0.0343	0.0436	0.0714
ω R ₂ [I>2 σ (I)]	0.0904	0.0917	0.1902
R ₁ (all data)	0.0391	0.0923	0.1066
ω R ₂ (all data)	0.0931	0.1233	0.2052
CCDC	1836801	1838721	1838722

Table S2. SOC coefficients of TA (unit: cm^{-1}).

	TA ^a	TA _{180°} ^b	TA _{opt-T} ^c
S ₀ -T ₁	7.4309	1.7009	1.7388
S ₁ -T ₁	5.9288	0.1261	1.8263×10^{-6}
S ₁ -T ₂	4.2865	1.2876	0.0065
S ₁ -T ₃	2.9359	0.5666	1.0249
S ₁ -T ₄	0.9536	0.9599	0.0014
S ₁ -T ₅	0.4986	0.1882	6.6481×10^{-7}
S ₁ -T ₆	3.7343	3.0761	0.0011
S ₁ -T ₇	1.9774	0.8246	0.0032
S ₁ -T ₈	3.1547	0.2018	0.1968
S ₁ -T ₉	7.9551	0.3027	0.7213
S ₁ -T ₁₀	1.8866	0.9757	2.8371×10^{-7}

^a Molecular structure is directly taken out from crystal structure. ^b TA_{180°} is the planar TA molecule which is factitiously constructed by Gaussuian09 software. ^c TA_{opt-T} is optimized T₁ geometry of TA by Gaussuian09 software.

Table S3. SOC coefficients of TA with different angles which are constructed by manually modulating molecular geometry in crystal (unit: cm^{-1}).

	100	110	120	130	140	150	160	170	180
S_0-T_1	3.5128	8.6739	3.4344	9.3337	10.2452	6.7250	3.2613	0.5395	1.7009
S_1-T_1	0.7390	10.5907	10.56527	5.84087	0.13497	0.1163	0.0754	0.0513	0.1261
S_1-T_2	1.2247	6.6144	0.7211	5.9544	6.6734	5.3383	4.0842	2.8347	1.2876
S_1-T_3	1.9319	1.1402	2.5846	2.6513	2.3411	1.9533	1.1540	0.6770	0.5666
S_1-T_4	1.0620	4.6094	2.8718	1.2483	1.1809	1.4848	1.6766	0.8843	0.9599
S_1-T_5	4.9270	0.9258	3.1675	0.1601	0.0467	0.0613	0.0642	0.0609	0.1882
S_1-T_6	5.3841	0.0855	0.5909	3.6530	3.3967	2.8874	2.2340	6.9332	3.0761
S_1-T_7	3.1944	1.0638	2.8328	1.1287	1.6729	1.6790	1.5827	1.4892	0.8246
S_1-T_8	6.1672	1.3318	4.7234	4.2335	3.2341	3.4112	10.1751	1.3225	0.2018
S_1-T_9	1.9671	4.5632	0.5886	6.7817	5.7773	10.4448	1.3128	0.3242	0.3027
S_1-T_{10}	6.3429	3.3612	6.0123	0.1664	2.7555	8.7551	2.9109	1.4938	0.9757

Table S4. Energy levels of TA with different angles which are constructed by manually modulating molecular geometry in crystal (unit: eV).

	100	110	120	130	140	150	160	170	180
S_1	4.9048	5.0562	4.9228	4.6805	4.4342	4.2119	4.0249	3.8843	3.8970
T_1	3.0760	3.3166	3.3032	3.2919	3.1718	3.0241	2.8742	2.7475	2.7468
T_2	3.3506	3.3293	3.3608	3.2949	3.2902	3.2952	3.3100	3.3297	3.3663
T_3	4.3271	4.4673	4.4702	4.4074	4.3082	4.1903	4.0567	3.9334	3.8994
T_4	4.4274	4.4937	4.4805	4.4248	4.3318	4.2093	4.0907	3.9944	3.9629
T_5	4.4414	4.5398	4.5100	4.4509	4.3506	4.2734	4.2201	4.1855	4.1830
T_6	4.4984	4.5856	4.5545	4.4867	4.4721	4.4696	4.4785	4.4534	4.3034
T_7	4.5093	4.6804	4.8245	4.8002	4.7073	4.6289	4.5779	4.4925	4.5191
T_8	4.5783	4.6982	4.8431	4.8478	4.8754	4.9143	4.7855	4.5489	4.5732
T_9	4.7714	4.8408	4.9135	5.0530	5.1572	5.1904	4.9743	5.0065	5.0528
T_{10}	4.8051	4.9459	4.9752	5.1354	5.3265	5.2733	5.2823	5.2897	5.2007

Table S5. SOC coefficients of TA with different angles based on optimized T_1 geometry (unit: cm^{-1}).

	100	110	120	130	140	150	160	170	180
S_0-T_1	5.7089	11.3511	8.6682	7.9181	5.7026	2.9059	0.7092	1.2239	1.7388

SV Tables

[1] H. Morita, Y. Oida, T. Ariga, S. Fukumoto, M. C. Sheikh, T. Fujii and T. Yoshimura, *Tetrahedron*, 2011, **67**, 4672.